Open Access Journal

Journal of Power Technologies 96 (1) (2016) 27–39

journal homepage:papers.itc.pw.edu.pl

High performances of Grid-connected DFIG based on Direct Power Control with Fixed Switching Frequency via MPPT Strategy using MRAC and Neuro-Fuzzy Control

Fayssal Amrane[a,*], Azeddine Chaiba[a], Saad Mekhilef[b]

[a] *University of Setif, Sétif 19000, Algeria, Department of Electrical Engineering, Automatic Laboratory of Sétif (LAS)*
[b] *University of Malaya, 50603 Kuala Lumpur, Malaysia, Department of Electrical Engineering, Power Electronics and Renewable Energy Research Laboratory (PEARL)*

Abstract

This paper presents high performance improved direct power control (DPC) based on model reference adaptive control (MRAC) and neuro-fuzzy control (NFC) for grid connected doubly fed induction generator (DFIG), to overcome the drawbacks of conventional DPC which was based only on PID controllers, namely the speed/efficiency trade-off and divergence from peak power under fast variation of wind speed. A mathematical model of DFIG implemented in the d-q reference frame is achieved. Then, a direct power control algorithm for controlling rotor currents of DFIG is incorporated using PID controllers, and space-vector modulation (SVM) is used to determine a fixed switching frequency. The condition of the stator side power factor is controlled at unity level via MPPT strategy. The MRAC which is based on DPC is investigated instead of PID regulators. Also, the performances of NFC based on DPC are tested and compared to those achieved using MRAC controller. The results obtained in the Matlab/Simulink environment using robustness tests show that the NFC is efficient, has superior dynamic performance and is more robust during parameter variations.

Keywords: Model reference adaptive control (MRAC), Neuro-Fuzzy Control (NFC), Wind energy conversion system (WECS), Doubly fed induction generator (DFIG), Direct power control (DPC), Space vector modulation (SVM), Maximum power point tracking (MPPT).

1. Introduction

Doubly-fed induction generator (DFIG) based wind energy conversion systems (WECSs) are mainly installed in remote and rural areas [1–3]. DFIG dominated wind power generation due to the outstanding advantages of the generator rating and lower converter cost [4]. A schematic diagram of a wind turbine system with a DFIG is shown in Fig. 1. For these reasons new control strategies were investigated in [5–8].

In most applications, the proportional-integral (PI) controller based Vector Control (VC) scheme is used to control DFIG in wind energy conversion systems [9, 10]. Although this control scheme is easy to implement, it has some drawbacks. One of the most important drawbacks of this control scheme is that the performance of the VC scheme largely depends on the tuning of the PI controller's parameters (K_p and K_i). Another drawback of this controller is that its performance also depends on the accuracy of the machine parameters and on grid voltage conditions such as harmonic level, distortion, etc. [10]. In order to improve the performance of the VC scheme, some studies have been proposed [11–16]. Control strategies of DFIG have been discussed in detail in the literature; Direct Power Control (DPC) [17, 18], Model Predictive Direct Power Control (MPDPC) [19, 20], Sliding mode Direct Power Control [21], Sliding mode control [22, 23] and Backstep-

*Corresponding author
Email addresses: amrane_fayssal@live.fr (Fayssal Amrane), chaiba_azeddine@yahoo.fr (Azeddine Chaiba), saad@um.edu.my (Saad Mekhilef)

ping Control [24].

More recently, the DPC technique has been proposed for DFIG based wind energy converion systems [5, 25–28]. In [26], the proposed technique requires the knowledge of the rotor and stator parameters to calculate the rotor flux at each sampling time. Therefore, the stability and robustness of this technique depend completely on the machine parameters. Also, the switching frequency of the converter is affected by power and speed variations. In [5], the control system is based on the stator flux position and the errors of the active and reactive powers. As the stator voltage waveform is relatively pure sinusoidal with constant frequency, the estimated stator flux accuracy is guaranteed. Thus, the control system is simple and the performance of the control system is independent of the machine parameters, except for stator resistance. However, the switching frequency of the converter is still affected significantly by active and reactive power variations and operating speed. A novel DPC strategy for the DFIG based wind energy generation system was presented in [27]. In this strategy, the required rotor voltage is directly calculated based on stator flux, rotor position, and errors of the active and reactive powers. To achieve constant switching frequency, a VSC and AC harmonic filter have been designed in this study. However, only simulation studies have been reported while the effects of sampling delay on the system have not been investigated.

MRAC is a kind of control method that follows the response signal at the output of reference model. It has the advantages of simple structure and fast and stable reconfiguration. The general idea underpinning MRAC is to incorporate a reference model to acquire the preferred closed-loop reactions. MRAC has the ability to control a system that undergoes parameter and/or environmental variations. It designs the mechanism law and adjustments technique to drive the desired trajectories for the system to track the reference model output [29, 30]. The analysis and performance of several model reference adaptive system (MRAS) observers for sensorless vector control of DFIG is proposed in [31]. A model reference adaptive control (MRAC) speed estimator for speed sensorless direct torque and flux control of an induction motor is proposed in [32] to achieve high performance sensorless drive.

Furthermore fuzzy-neural techniques have been proposed as a robust control for electrical drives [33–35]. Neuro-fuzzy systems combine the advantages of neural networks and fuzzy logic systems. The main purpose of using the ANFIS (Adaptive Neuro-Fuzzy Inference Systems) approach is to automatically deliver the fuzzy system by using neural network methods [36, 37]. The ANFIS architecture has well known advantages of modeling a highly non-linear system, as it combines the capability of fuzzy reasoning in handling the uncertainties and capability of an artificial neural network (ANN) in learning from processes. A combination of the strengths of Fuzzy Logic controllers and Neural Networks creates systems capable of controlling complex systems and adaptively learning to optimize control parameters [36, 37]. These advantages justify the necessity of applying this kind of system for the DFIG used in wind energy conversion systems.

In this paper the main contribution is the validation of the proposed DPC based on robust controllers MRAC and NFC with/without MPPT strategy instead of conventional DPC which is based only on PID controllers, by using robustness tests, in terms of: reference tracking, overshoot, active and reactive power error and THD of stator current injected to the grid. To extract the maximum power despite sudden variations in wind speed, we used the maximum power point tracking (MPPT) strategy, stator active power is extracted from wind power and stator reactive power is maintained at zero level to ensure unity power.

This paper is organized as follows; the model of the turbine is presented in section 2. In section 3, the mathematical model of DFIG is given. Section 4 presents Direct Power Control of DFIG which is based on the orientation of the stator flux vector along the d axis. Model Reference Adaptive Control (MRAC) and Neuro-Fuzzy Control (NFC) are established to control the rotor currents and are presented in sections 5 and 6 respectively. In section 7, simulation results are given and discussed.

2. Model of the Turbine

The wind turbine input power is usually:

$$Pv = \frac{1}{2} \cdot \rho \cdot S_w \cdot v^3 \tag{1}$$

where ρ is air density; S_w is wind turbine blades swept area in the wind; v is wind speed.

The output mechanical power of wind turbine is:

$$P_m = C_p \cdot P_v = \frac{1}{2} \cdot \rho \cdot S_w \cdot v^3 \tag{2}$$

where Cp represents the wind turbine power conversion efficiency. It is a function of the tip speed ratio λ and the

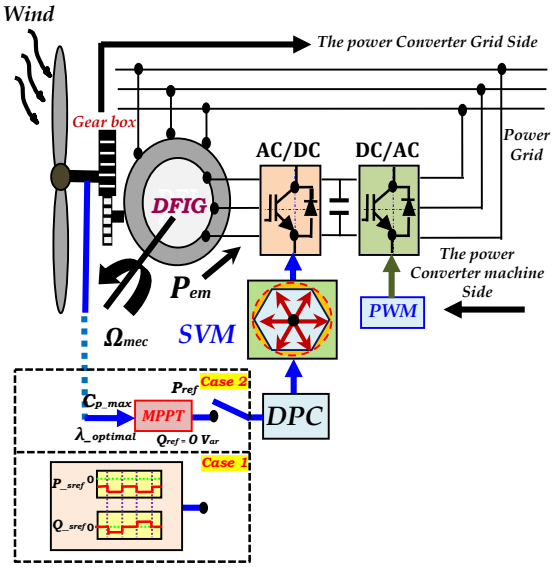

Figure 1: Schematic diagram of wind turbine system with a DFIG

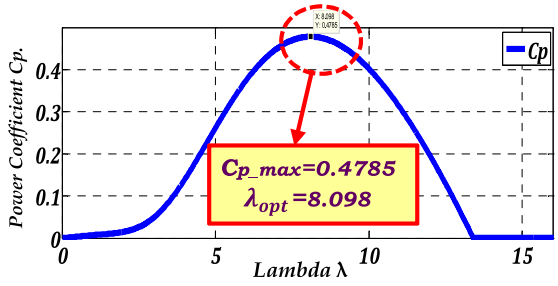

Figure 2: Aerodynamic power coefficient variation Cp against tip speed ratio λ and pitch angle β

blade pitch angle β in a pitch-controlled wind turbine. λ is defined as the ratio of the tip speed of the turbine blades to wind speed. λ is given by:

$$\lambda = \frac{R \cdot \Omega_t}{\nu} \tag{3}$$

where R is blade radius, Ω_t is angular speed of the turbine. C_p can be described as [23, 24]:

$$Cp = (0.5 - 0.0167 \cdot (\beta - 2)) \cdot sin\left[\frac{\pi \cdot (\lambda + 0.1)}{18.5 - 0.3 \cdot (\beta - 2)}\right] - 0.00184 \cdot (\lambda - 3) \cdot (\beta - 2) \tag{4}$$

The maximum value of C_p ($C_{p_{max}} = 0.4785$) is achieved for $\beta = 0$ degree and for $\lambda opt = 8.098$. This point corresponds at the maximum power point tracking (MPPT) [38, 39]

After the simulation of the wind turbine using this wind profile, we test the robustness of our MPPT algorithm and obtain the curve of power coefficient Cp versus time; this latter achieved the maximum value mentioned

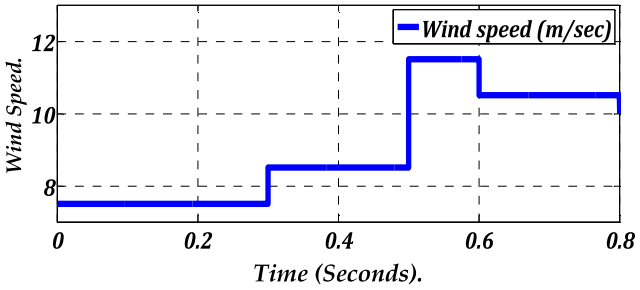

Figure 3: Wind profile (Wind speed)

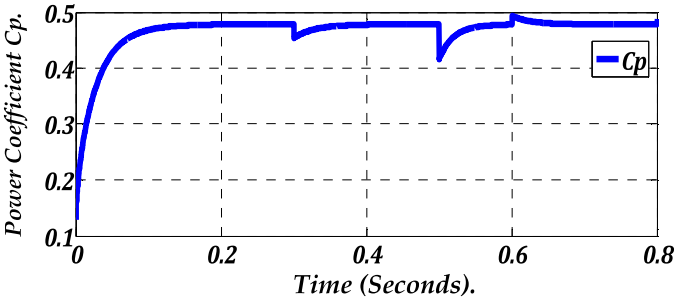

Figure 4: Power coefficient (Cp)

in Fig. 2 ($Cp_{max} = 0.4785$) despite the variation of the wind [38].

3. Mathematical Model of DFIG

The generator chosen for the conversion of wind energy is a double-fed induction generator, DFIG modeling described in the two-phase reference (Park). The general electrical state model of the induction machine obtained using Park transformation is given by the following equations, [40–42]:

Stator and rotor voltages:

$$V_{sd} = R_s * I_{sd} + \frac{d}{dt}\phi_{sd} - \omega_s * \phi_{sq} \tag{5}$$

$$V_{sq} = R_s * I_{sq} + \frac{d}{dt}\phi_{sq} + \omega_s * \phi_{sd} \tag{6}$$

$$V_{rd} = R_r * I_{rd} + \frac{d}{dt}\phi_{rd} - (\omega_s - \omega) * \phi_{rq} \tag{7}$$

$$V_{rq} = R_r * I_{rq} + \frac{d}{dt}\phi_{rq} - (\omega_s - \omega) * \phi_{rd} \tag{8}$$

Stator and rotor fluxes:

$$\phi_{sd} = L_s * I_{sd} + L_m * I_{rd} \tag{9}$$

$$\phi_{sq} = L_s * I_{sq} + L_m * I_{rd} \tag{10}$$

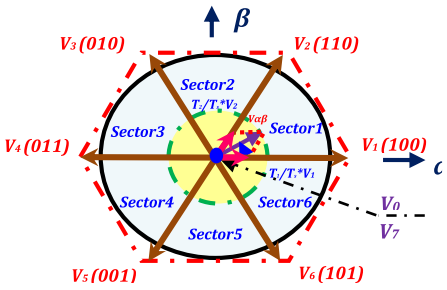

Figure 5: The diagram of voltage space vectors in α-β plan

$$\phi_{rd} = L_r * I_{rd} + L_m * I_{sd} \tag{11}$$

$$\phi_{rq} = L_r * I_{rq} + L_m * I_{sd} \tag{12}$$

The electromagnetic torque is given by:

$$Ce = P * L_m * (I_{rd} * I_{sq} - I_{rq} * I_{sd}) \tag{13}$$

And its associated motion equation is:

$$Ce - Cr = J * \frac{d}{dt}\Omega + f * \Omega \tag{14}$$

$$J = \frac{J_{turbine}}{G^2} + Jg \tag{15}$$

where: Cr is the load torque J is total inertia in DFIG's rotor, Ω is mechanical speed and G is gain of the gear box.

The voltage vectors, produced by a three-phase PWM inverter, divide the space vector plane into six sectors, as shown in Fig. 5 [39].

In every sector (Fig. 6), each voltage vector is synthesized by the basic space voltage vector of the 2 sides of the sector and 1 zero vector. For example, in the first sector, $V_{\alpha\beta}$ is a synthesized voltage space vector and is expressed by:

$$\overrightarrow{V_{\alpha\beta}} = \frac{T_1}{T_s} \cdot \overrightarrow{V_1} + \frac{T_1}{T_s} \cdot \overrightarrow{V_2} \tag{16}$$

4. Direct Power Control of DFIG

In this section, the DFIG model can be described by the following state equations in the synchronous reference frame whose d axis is aligned with the stator flux vector as shown in Fig. 7, $\phi_{sd} = \phi_s$ and ϕ_{sq} [29].

By neglecting resistances of the stator phases, the stator voltage will be expressed by:

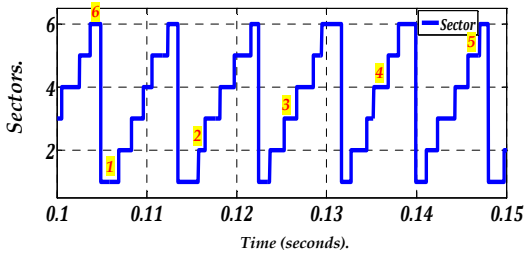

Figure 6: Sectors of space vector modulation (SVM) approach

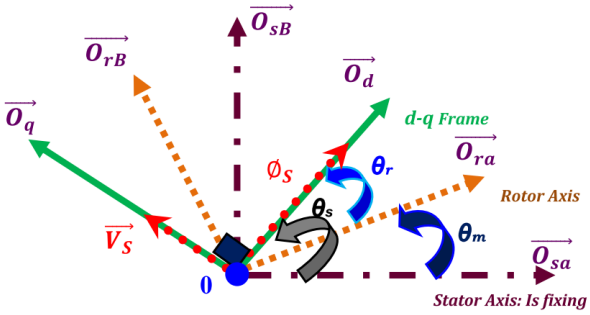

Figure 7: Stator and rotor flux vectors in the synchronous d-q Frame

$$V_{sd} = 0 \quad \text{and} \quad V_{sq} = V_S \cong \omega_S \cdot \phi_S \text{ and} \tag{17}$$

We lead to an uncoupled power control where the transversal component i_{rq} of the rotor current controls the active power. The reactive power is imposed by the direct component i_{rd} as shown in Fig. 8:

$$Ps = -Vs * \frac{Lm}{Ls} * Irq \tag{18}$$

$$Qs = \frac{V_s^2}{\omega_{s*} Ls} - Vs * \frac{Lm}{Ls} * Ird \tag{19}$$

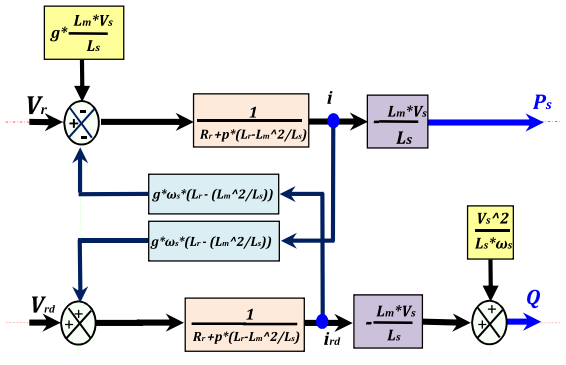

Figure 8: The Doubly Fed Induction Generator simplified model

The arrangement of the equations gives the expressions of the voltages according to the rotor currents:

$$Vrd = Rr * Ird + (Lr - \frac{Lm^2}{Ls}) * \frac{dIrd}{dt} - g * \omega_s * (Lr - \frac{Lm^2}{Ls}) * Irq \quad (20)$$

$$Vrq = Rr * Irq + (Lr - \frac{Lm^2}{Ls}) * \frac{dIrq}{dt} + g * \omega_s * (Lr - \frac{Lm^2}{Ls}) * Irq + g * \frac{Lm * Vs}{Ls} \quad (21)$$

$$Ird = -\frac{1}{\sigma * \tau_r} * Ird + g * \omega_s * Irq + \frac{1}{\sigma * Lr} * Vrd \quad (22)$$

$$Irq = -\frac{1}{\sigma} * (\frac{1}{\tau_r} + \frac{L_m^2}{Ls * Ts * Lr}) * Irq - g * \omega s * Ird + \frac{1}{\sigma * Lr} * Vrq \quad (23)$$

$$Tr = \frac{Lr}{Rr}; Ts = \frac{Ls}{Rr}; \sigma = 1 - \frac{L_m^2}{Ls * Lr} \quad (24)$$

where:
ϕ_{sd}, ϕ_{sq}, are stator flux components, ϕ_{rd}, $\phi_{rq}$are rotor flux components, V_{sd}, V_{sq} are stator voltage components, V_{rd}, V_{rq}, are rotor voltage components. R_s, R_r are stator and rotor resistances, L_s, L_r are stator and rotor inductances, L_m is mutual inductance, σ is leakage factor, P is number of pole pairs, ωs is the stator pulsation, ω is the rotor pulsation, f is the friction coefficient, T_s and T_r are stator and rotor time-constant, and g is the slid.

5. Model Reference Adaptive Control (MRAC)

MRAC is a kind of control method that follows the response signal at the output of the reference model. It has the advantages of simple structure and fast and stable reconfiguration. The general idea underpinning MRAC is to incorporate a reference model to acquire the preferred closed-loop reactions. MRAC designs the mechanism law and adjustments technique to drive the desired trajectories for the system to track the reference model output [29, 30]. The block diagram of the MRAC is shown in Fig. 9. As seen from the figure, the basic MRAC observer consists of two independent models for estimating the same parameter. One is called the reference model, and this model does not include an estimated parameter, and the other is called an adjustable

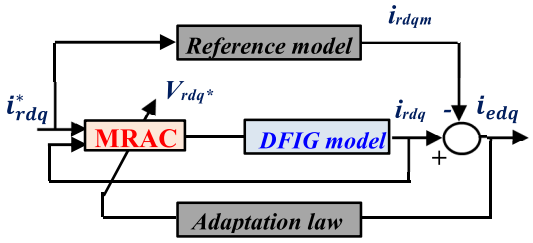

Figure 9: Model reference adaptive control

model, which depends entirely on the estimated parameter.

The system studied in this paper can be specified by a first-order model given by the outputs of rotor current controllers as:

$$\frac{di_{rd}}{dt} = -a \cdot i_{ird} + b \cdot V^r_{rd} \quad (25)$$

$$\frac{di_{rq}}{dt} = -a \cdot i_{irq} + b \cdot V^r_{rq} \quad (26)$$

where i_{rdq} is the system state, a and b are the system model parameters, V^r_{rd} is the control signal. This last is defined as:

$$V^r_{rd} = K(t) \cdot i_{rdq} + Kr(t) \cdot i_{rdq} \quad (27)$$

where: i^*_{rdq} is the reference signal, $K(t)$ and $Kr(t)$ are the feedback and the feed forward gain respectively. For controlling the system, the outputs of rotor current controller may be rewritten as follows [30]:

$$\frac{di_{rdqm}}{dt} = a \cdot i_{rdqm} + b_m \cdot i^*_{rdq} \quad (28)$$

where i_{rdqm} is the state of the reference model, a_m and b_m are the reference model parameters. The dynamics of the system may be written as:

$$\frac{di_{edq}}{dt} = a_m \cdot i_{edq} + (a - a_m - b \cdot K(t)) \cdot i_{rdq} + (b_m - b \cdot Kr(t)) \cdot i^*_{rdq} \quad (29)$$

where $i_{edq} = i_{rdqm} - i_{rdq}$ is the error signal. Using Equations 27, 28 and 29, it can be seen that for exact matching between the system and the reference model, the next expressions:

$$k = k^E = \frac{a - am}{b} \quad (30)$$

$$kr = k^E_r = \frac{bm}{b} \quad (31)$$

where $(\,)^E$denotes the (constant) Erzberger gains.

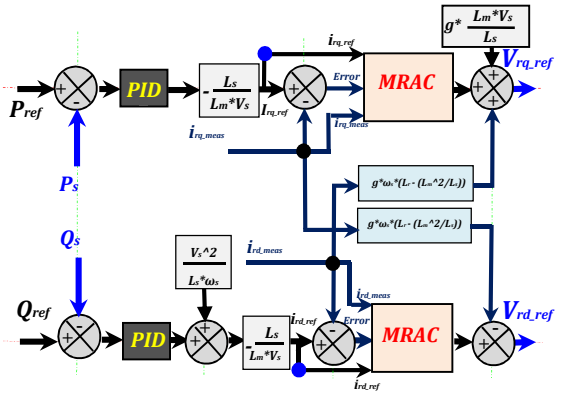

Figure 10: The proposed DPC based on MRAC

Equations (30) and (31) can be used to express Equation (29) as:

$$\frac{di_{edq}}{dt} = -am \cdot i_{edq} + (K^E - K) \cdot (i_{rdqm} - i_{edq}) + (K^E - K) \cdot i_{rdq} \quad (32)$$

For universal MRAC, the adaptive gains are usually expressed as given below [30]:

$$k(e,t) = \int_0^t a \cdot ye \cdot I_{rdq}^T \cdot dt + \beta \cdot ye \cdot I_{rdq}^T \quad (33)$$

$$kr(e,t) = \int_0^t a \cdot ye \cdot I_{rdqref}^T \cdot dt + \beta \cdot ye \cdot I_{rdqref}^T \quad (34)$$

where α and β are adaptive control weightings representing the adaptive effort, y_e is a scalar weighted function of the error state and its derivatives, $y_e = c_e \cdot x_e$ where c_e can be chosen to ensure the stability of the feed forward block.
The proposed DPC of a DFIG based on MRAC is shown in Fig. 10.

6. Design of Neuro-Fuzzy Controller

The block diagram of the neuro-fuzzy controller (NFC) system is shown in Fig. 11. The NFC controller is composed of an on-line learning algorithm with a neuro-fuzzy network. The neuro-fuzzy network is trained using an on-line learning algorithm. The NFC has two inputs, the rotor current error e_{idr} and the derivative of rotor current error e'_{idr}.

The output is rotor voltage v_{dr}. For the NFC of rotor current i_{qr} is similar to i_{dr} controller [34, 35].

The current error (as shown in Fig. 13) and its variation are sampled and fuzzified according to pre-decided fuzzy rules. The training procedure of NFC is based on

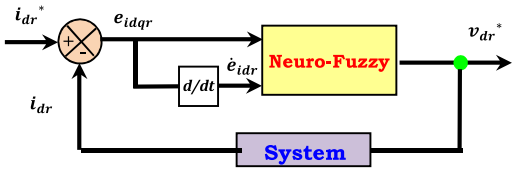

Figure 11: Block diagram of the neuro-fuzzy controller

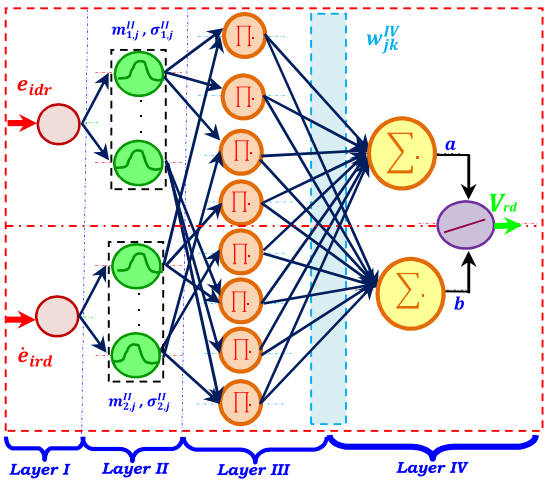

Figure 12: Schematic diagram of the neuro-fuzzy network.

FLC. For the NFC, a four layer NN as shown in Fig. 12 is used. Layers I–IV represents the inputs of the network, the membership functions, the fuzzy rule base and the outputs of the network, respectively [33–35].

6.1. A.1- Layer I: Input layer

Inputs and outputs of nodes in this layer are represented as:

$$net_1^I = eird(t), y_1^I = f_1^I(net_1^I) = net_1^I = eird(t) \quad (35)$$

$$net_2^I = e'ird(t), y_2^1 = f_2^I(net_2^I) = net_2^I = e'ird(t) \quad (36)$$

6.2. A.2- Layer II: membership layer

In this layer, each node performs a fuzzy set and the Gaussian function is adopted as a membership function.

6.3. A.3- Layer III: rule layer

This layer includes the rule base used in the fuzzy logic control (FLC). Each node in this layer multiplies the input signals and outputs the result of product.

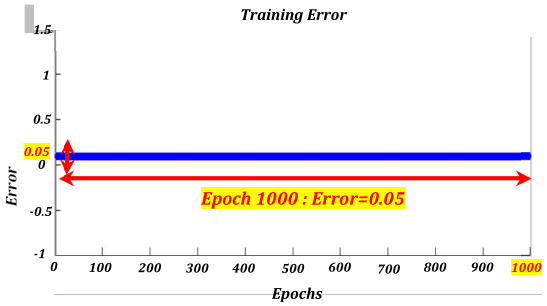

Figure 13: Rotor current error (Matlab/Simulink interface)

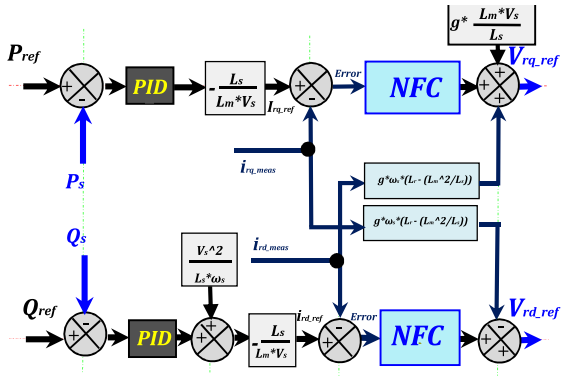

Figure 14: Proposed DPC based on NFC

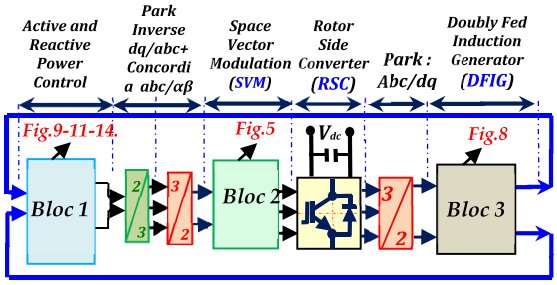

Figure 15: Global System

6.4. A.4. Layer IV: output layer

This layer represents the inference and defuzzification used in the FLC. For defuzzification, the center of area method is used.

In this work, the NFC parameters are chosen as follows:

- Takagi Sugeno Type;
- N° of iteration is 500;
- Error tolerance is $5 \cdot 10^{-3}$;
- Epochs are 1000;
- N° of membership functions is 7;
- N° of hidden layer neurons is 14;

The number of neurons in the input and output layers is defined by the number of inputs and outputs required by the application, respectively. There are no general guidelines for defining the best number of neurons in the hidden layer.

The proposed DPC of a DFIG based on NFC is shown in Fig. 14.

The overall system is described in detail, as shown in Fig. 15.

7. Simulation Results and Discussion

Fig. 11 and Fig. 14 show the block diagram of the proposed DPC based on MRAC and NFC respectively. The results, reported in Figs. 16 to 37, were used to investigate system behavior during power tracking. DFIG used in this work is 4 kW and its nominal parameters are indicated in Table. 3. The wind turbine is 10 kW and its parameters are indicated in Table 4. In case 1, we simulate a proposed control based on MRAC and NFC (Fig. 11 and Fig. 14) using the Matlab/Simulink environment, without a Maximum Power Point Tracking (MPPT) strategy.

7.1. Case 1 (Without MPPT Strategy):

The stator active and reactive powers and its reference profiles are presented in Fig. 16, its reference are indicated in Table 5. It is clear that the measured powers (active and reactive) have good tracking with high performances (little error, and short response time) compared to their reference powers in transient and steady states. I_{r_abc} and I_{r_abc} are shown in Fig. 17 and Fig. 18 respectively, we remark the sinusoidal form of the three rotor and stator currents. I_{rd}, I_{rd} and ϕ_{rd}, ϕ_{rq} are presented respectively in Fig. 19 and Fig. 21, they present the inverse diagrams compared to reactive and active powers. The inverse for I_{sd}, I_{sd}, they have the same diagrams of reactive and active powers. The tracking errors of active and reactive powers are shown in Fig. 22. We observe a low power error:

$$-100W/Var \leq \triangle Ps \ \triangle Qs \leq +100W/Var$$

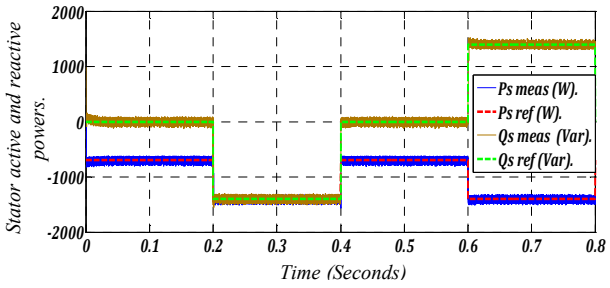

Figure 16: Stator active and reactive powers

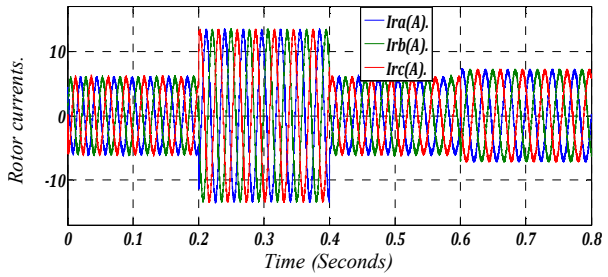

Figure 17: Rotor currents Ir_abc.

We use a robustness test for both cases (Proposed DPC based on MRAC and NFC), as follows:

- Test 1: (Without robustness test)→Blue color.
- Test 2: Add 100% for Rr, and decrease 25% for Ls, Lr, and Lm respectively→ Brown color.
- Test 3: Add 100% for Rr and J, and decrease 25% for Ls, Lr, and Lm→ Green color

The stator active powers and its reference profiles for proposed controls based on MRAC and NFC are presented in Fig. 23 and Fig 25 respectively. We note that the stator active powers follow exactly its references for both proposed controls (Test1-blue color). After a robustness test (Test 2-brown color), the stator active powers follow its references, but we note that there is a great power error and more ripples in the proposed

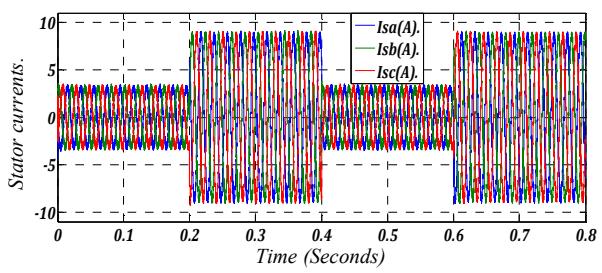

Figure 18: Stator currents Is_abc

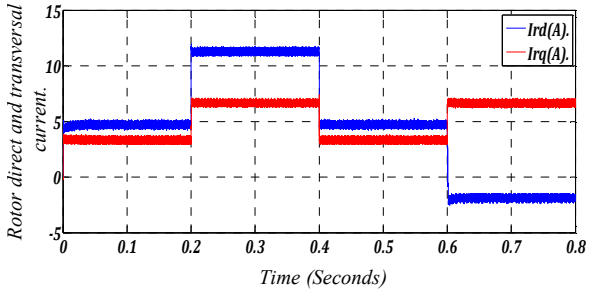

Figure 19: Rotor direct current and rotor transversal current

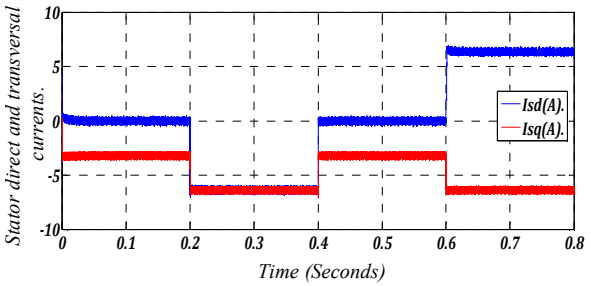

Figure 20: Stator direct current and stator transversal current

control based on MRAC, and neglected in NFC. After adding 100% of the moment inertia J, severe disruptions are noted (Test3-green color) just for the proposed control based on MRAC because it is influenced by parameter variation. The stator reactive powers and its reference profiles for proposed controls based on MRAC and NFC are presented in Fig. 24 and Fig 26 respectively. We note the stator reactive powers follow exactly its references for both proposed controls (Test1-blue color). By using a robustness test (Test2-brown color) and (Test 3-green color), we note lower undulations in the proposed control based on MRAC and neglected in NFC, we note also a little overshoot in the proposed control based on MRAC and neglected in NFC. The overshoot existence, the THD of the stator and rotor current and the value of the active and reactive power errors (only for test 1-Blue color), are

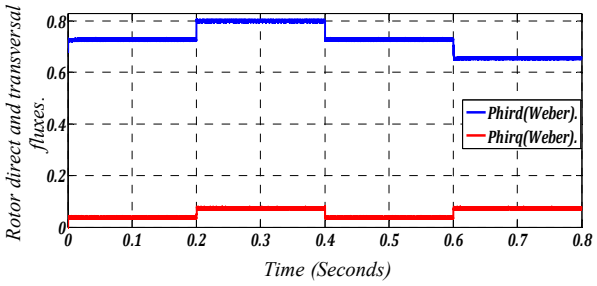

Figure 21: Rotor direct flux and rotor transversal flux

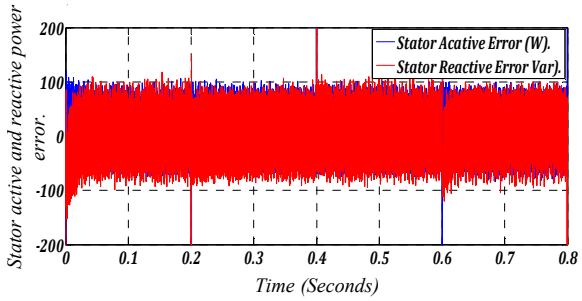

Figure 22: Stator active and reactive power error

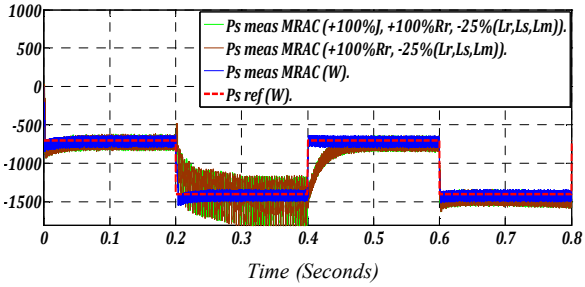

Figure 23: Stator active power based on MRAC

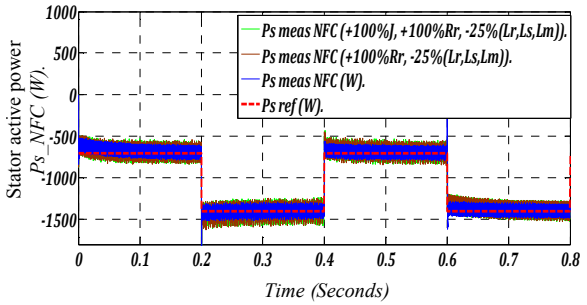

Figure 25: Stator active power based on NFC

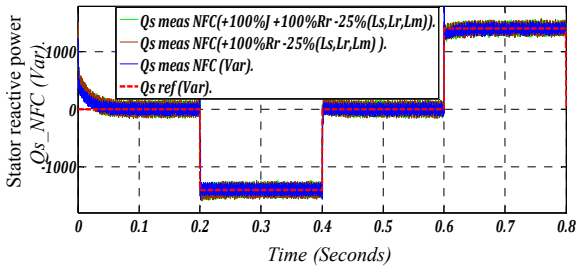

Figure 26: Stator reactive power based on NFC

mentioned in table 1.

In case 2, we simulate both the proposed control based on MRAC and NFC (Fig. 11 and Fig. 14) using the Matlab/Simulink§environment, with Maximum Power Point Tracking (MPPT) strategy.

7.2. Case 2 (With MPPT Strategy):

The stator active and reactive powers and its reference profiles are presented in Fig. 27. The stator active power reference is extracted from MPPT strategy; it takes the inverse diagram of wind speed. The stator reactive power equal to 0 Var, represents power factor unity. It is clear that the measured powers (active and reactive) have good tracking with high performances (little error, and short response time) compared to their reference powers in transient and steady states. I_{r_abc}, I_{s_abc} are presented respectively in Fig. 28 and Fig. 29. We note the sinusoidal form of the three phases of rotor and stator currents. I_{rd}, I_{rq} and ϕ_{rd}, ϕ_{rq} are presented respectively in Fig. 30 and Fig. 32, they represent the inverse diagrams of reactive and active powers respectively. And the inverse for Fig. 31 I_{sd}, I_{sq} have the same diagrams of reactive and active powers respectively. The tracking error of active and reactive powers is shown in Fig. 33. We observe a low power error of active and reactive powers: $-80W/Var \leq \triangle Ps\ \triangle Qs \leq +80W/Var$ Except between 0.5 and 0.7 sec $-80W/Var \leq \triangle Ps\ \triangle Qs \leq +80W/Var$

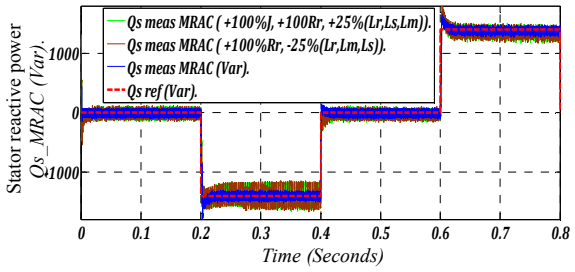

Figure 24: Stator reactive power based on MRAC

Table 1: Result's Recapitulation

	Proposed Control	
	Based on MRAC	Based on NFC
Overshoot	A little	Neglected
Stator Current's THD	0.81 %	0.78 %
Rotor Current's THD	17.01 %	2.80 %
Power's error	+/- 100 (W_VAR)	+/- 100 (W_VAR)

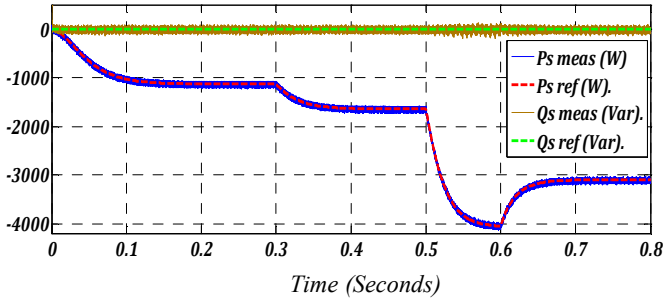

Figure 27: Stator active and reactive powers

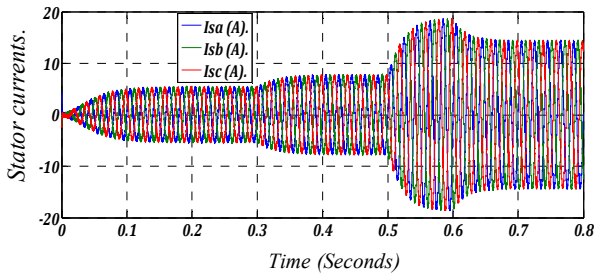

Figure 28: Stator currents Is_abc

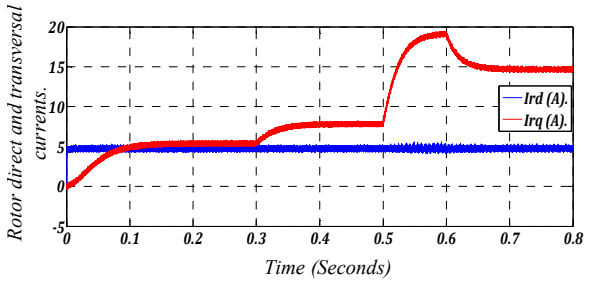

Figure 30: Rotor direct current and rotor transversal current

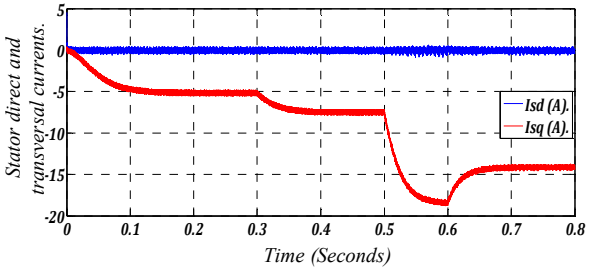

Figure 31: Stator direct current and stator transversal current

For both cases (Proposed DPC based on MRAC and NFC) we use a robustness test as follows:

- Test 1: (Without robustness test)→Blue color.
- Test 2: Add 100 % for Rr, and decrease 25 % for Ls, Lr, and Lm→ Brown color.
- Test 3: Add 100 % for Rr and J, and decrease 25 % for Ls, Lr, and Lm→ Green color

The stator active powers injected into the grid for proposed controls based on MRAC and NFC via MPPT strategy are presented in Fig. 34 and Fig. 36 respectively. We note that the stator active powers follow exactly its references in transient and steady states, for both proposed controls (Test1-blue color). After a robustness test (Test 2-brown color), the stator active powers follow its references, but we note that there are few ripples in the proposed MRAC especially between 0.5 sec and 0.7 sec and neglected in NFC. After adding +100% of the moment inertia J, a remarkable power error is noted (nearly +/-200 W) with severe disruptions; this is only in the proposed control using MRAC (Test3-green color) because it is influenced by parameter variation. The stator reactive powers injected into the grid for the proposed controls using MRAC and NFC via MPPT strategy are presented in Fig. 35 and Fig. 37 respectively. We note that the stator reactive powers follow exactly its reference (0 Var- Power Factor Unity) in transient and steady states for both proposed controls (Test1-blue color). By using a robustness test (Test2-brown color) and (Test 3-green color), we note a remarkable power error (nearly +/- 700 Var) especially between 0.5 sec and 0.8 sec, with severe disruptions and more ripples in the proposed control based on MRAC (doesn't maintain 0 Var) and power factor (PF) is dif-

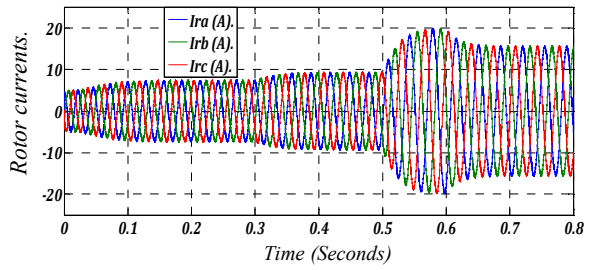

Figure 29: Rotor currents Ir_abc

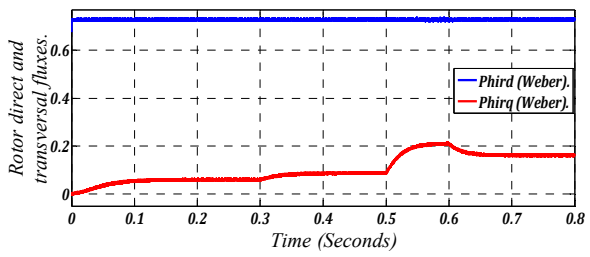

Figure 32: Rotor direct flux and rotor transversal flux

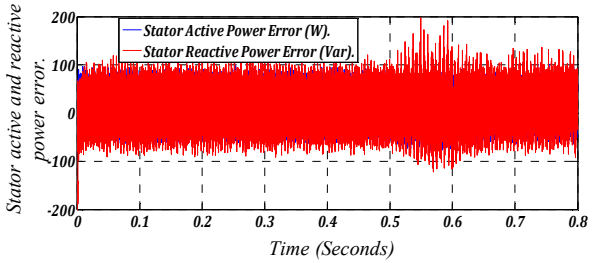

Figure 33: Stator active and reactive power error

ferent than unity, and neglected in the proposed control based on NFC. The overshoot existence, the THD of the stator and rotor current and the value of the active and reactive power errors (only for test 1-Blue color), are mentioned in table 2.

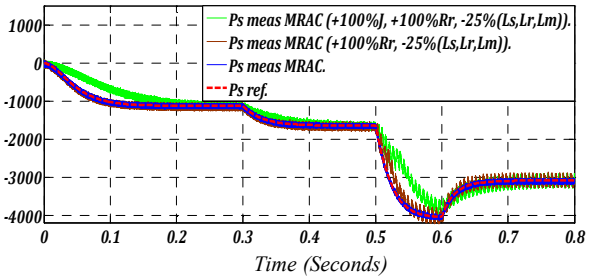

Figure 34: Stator active power based on MRAC

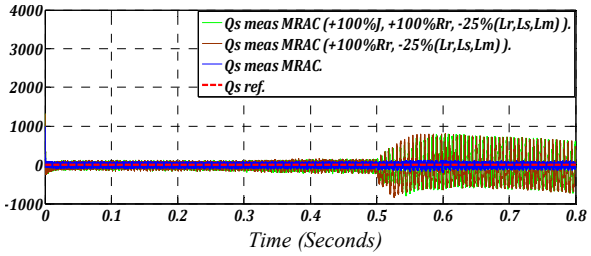

Figure 35: Stator reactive power based on MRAC

Table 2: Result Recapitulation

	Proposed Control	
	Based on MRAC	Based on NFC
Overshoot	Neglected	Neglected
Stator Current's THD	1.01%	0.99%
Rotor Current's THD	24.64%	18.42%
Power's error	+/- 120 (W_VAR)	+/- 120 (W_VAR)

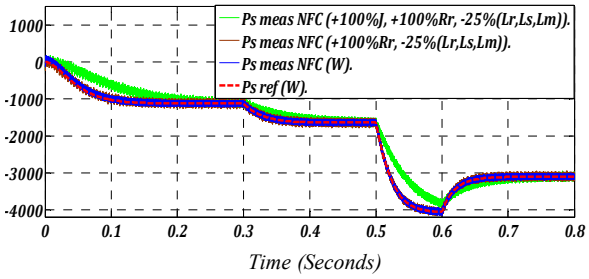

Figure 36: Stator active power based on NFC

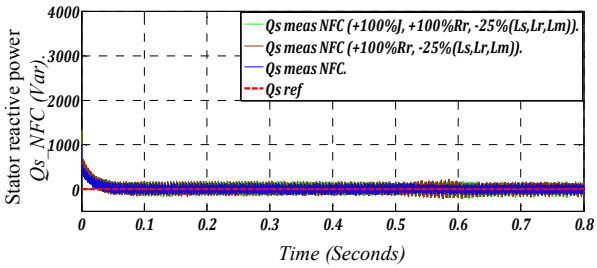

Figure 37: Stator reactive power based on NFC

Table 3: Parameters of the DFIG.

Rated Power:	4 kWatts
Stator Resistance:	Rs = 1.2Ω
Rotor Resistance:	Rr = 1.8Ω
Stator Inductance:	Ls = 0.1554 H.
Rotor Inductance:	Lr = 0.1558 H.
Mutual Inductance:	Lm = 0.15 H.
Rated Voltage:	Vs = 220/380 V
Number of Pole pairs:	P= 2
Rated Speed:	N=1440 rpm
Friction Coefficient:	fDFIG=0.00 N·m/sec
The moment of inertia	J=0.2 kg·m^2
Slip:	g=0.015

Table 4: Parameters of the Turbine.

Rated Power:	10 kWatts
Number of Pole pairs:	P= 3
Blade diameter	R= 3m
Gain:	G=3.9
The moment of inertia	Jt=0.00065 kg·m^2
Friction coefficient	ft=0.017 N·m/sec
Air density:	ρ=1.22 Kg/m^3

Table 5: Active and Reactive Power References.

Time (sec):	Stator Active Power	Stator Reactive Power
[0 - 0.2].	-700 Watts.	0 Var.
[0.2 - 0.4].	-1400 Watts.	-1400 Var.
[0.4 - 0.6].	-700 Watts.	0 Var.
[0.6 - 0.8].	-1400 Watts.	+1400 Var.

8. Conclusion

This paper presents the high performances of an improved direct power control based on MRAC and Neuro-fuzzy control for grid connection doubly fed induction generator. In order to control the DFIG, direct power control with SVM has been achieved by adjusting active and reactive powers and rotor currents. The performances of NFC based on DPC were tested and compared to those achieved using the MRAC controller. Simulation results obtained in the Matlab/Simulink environment using robustness tests via MPPT strategy have shown that the NFC is efficient, has superior dynamic performance and is more robust during parameter variations.

[1] J. Mohammadi, S. Vaez-Zadeh, S. Afsharnia, E. Daryabeigi, A combined vector and direct power control for dfig-based wind turbines, Sustainable Energy, IEEE Transactions on 5 (3) (2014) 767–775.

[2] A. A. B. M. Zin, M. P. HA, A. B. Khairuddin, L. Jahanshaloo, O. Shariati, An overview on doubly fed induction generators controls and contributions to wind based electricity generation, Renewable and Sustainable Energy Reviews 27 (2013) 692–708.

[3] R. Cárdenas, R. Peña, S. Alepuz, G. Asher, Overview of control systems for the operation of dfigs in wind energy applications, IEEE Transactions on Industrial Electronics 7 (60) (2013) 2776–2798.

[4] M. F. Iacchetti, G. D. Marques, R. Perini, A scheme for the power control in a dfig connected to a dc bus via a diode rectifier, Power Electronics, IEEE Transactions on 30 (3) (2015) 1286–1296.

[5] H. Nian, Y. Song, Direct power control of doubly fed induction generator under distorted grid voltage, Power Electronics, IEEE Transactions on 29 (2) (2014) 894–905.

[6] P. Gayen, D. Chatterjee, S. Goswami, Stator side active and reactive power control with improved rotor position and speed estimator of a grid connected dfig (doubly-fed induction generator), Energy 89 (2015) 461–472.

[7] R. D. Shukla, R. K. Tripathi, Isolated wind power supply system using double-fed induction generator for remote areas, Energy Conversion and Management 96 (2015) 473–489.

[8] R. D. Shukla, R. K. Tripathi, A novel voltage and frequency controller for standalone dfig based wind energy conversion system, Renewable and Sustainable Energy Reviews 37 (2014) 69–89.

[9] R. Cárdenas, R. Peña, S. Alepuz, G. Asher, Overview of control systems for the operation of dfigs in wind energy applications, IEEE Transactions on Industrial Electronics 7 (60) (2013) 2776–2798.

[10] E. Tremblay, S. Atayde, A. Chandra, Comparative study of control strategies for the doubly fed induction generator in wind energy conversion systems: a dsp-based implementation approach, Sustainable Energy, IEEE Transactions on 2 (3) (2011) 288–299.

[11] B. Pimple, V. Vekhande, B. Fernandes, A new direct torque control of doubly-fed induction generator under unbalanced grid voltage, in: Applied Power Electronics Conference and Exposition (APEC), 2011 Twenty-Sixth Annual IEEE, IEEE, 2011, pp. 1576–1581.

[12] A. Hassan, A. El-Sawy, O. Kamel, Direct torque control of a doubly fed induction generator driven by a variable speed wind turbine, Journal of Engineering Sciences, Assiut University 41 (1) (2013) 199–216.

[13] H. Fathabadi, Control of a dfig-based wind energy conversion system operating under harmonically distorted unbalanced grid voltage along with nonsinusoidal rotor injection conditions, Energy Conversion and Management 84 (2014) 60–72.

[14] J. Hu, X. Yuan, Vsc-based direct torque and reactive power control of doubly fed induction generator, Renewable energy 40 (1) (2012) 13–23.

[15] R. Abdelli, D. Rekioua, T. Rekioua, A. Tounzi, Improved direct torque control of an induction generator used in a wind conversion system connected to the grid, ISA transactions 52 (4) (2013) 525–538.

[16] M. V. Kazemi, A. S. Yazdankhah, H. M. Kojabadi, Direct power control of dfig based on discrete space vector modulation, Renewable Energy 35 (5) (2010) 1033–1042.

[17] M. K. Bourdoulis, A. T. Alexandridis, Direct power control of dfig wind systems based on nonlinear modeling and analysis, Emerging and Selected Topics in Power Electronics, IEEE Journal of 2 (4) (2014) 764–775.

[18] K. Äström, B. Wittenmark, Adaptive control, NY: Addison-Wesley.

[19] J. Hu, J. Zhu, D. G. Dorrell, Predictive direct power control of doubly fed induction generators under unbalanced grid voltage conditions for power quality improvement, Sustainable Energy, IEEE Transactions on 6 (3) (2015) 943–950.

[20] J. Hu, J. Zhu, D. G. Dorrell, Model-predictive direct power control of doubly-fed induction generators under unbalanced grid voltage conditions in wind energy applications, Renewable Power Generation, IET 8 (6) (2014) 687–695.

[21] E. Shehata, Sliding mode direct power control of rsc for dfigs driven by variable speed wind turbines, Alexandria Engineering Journal 54 (4) (2015) 1067–1075.

[22] S. Taraft, D. Rekioua, D. Aouzellag, S. Bacha, A proposed strategy for power optimization of a wind energy conversion system connected to the grid, Energy Conversion and Management 101 (2015) 489–502.

[23] M. DOUMI, A. G. AISSAOUI, A. TAHOUR, M. ABID, Commande adaptative d'un système éolien, Rev. Roum. Sci. Techn. Électrotechn. Et Énerg. 60 (1) 99–110.

[24] B. Bossoufi, M. Karim, A. Lagrioui, M. Taoussi, A. Derouich, Observer backstepping control of dfig-generators for wind turbines variable-speed: Fpga-based implementation, Renewable Energy 81 (2015) 903–917.

[25] L. Xu, P. Cartwright, Direct active and reactive power control of dfig for wind energy generation, Energy Conversion, IEEE Transactions on 21 (3) (2006) 750–758.

[26] D. Zhi, L. Xu, Direct power control of dfig with constant switching frequency and improved transient performance, Energy Conversion, IEEE Transactions on 22 (1) (2007) 110–118.

[27] S. Demirbas, S. Bayhan, Active and reactive power control of doubly fed induction generator using direct power control technique, in: Power Engineering, Energy and Electrical Drives (POWERENG), 2013 Fourth International Conference on, IEEE, 2013, pp. 41–45.

[28] M. Farshadnia, S. A. Taher, Current-based direct power control of a dfig under unbalanced grid voltage, International Journal of Electrical Power & Energy Systems 62 (2014) 571–582.

[29] G. D. Marques, M. F. Iacchetti, Stator frequency regulation in a field-oriented controlled dfig connected to a dc link, Industrial Electronics, IEEE Transactions on 61 (11) (2014) 5930–5939.
[30] S. Abdeddaim, A. Betka, S. Drid, M. Becherif, Implementation of mrac controller of a dfig based variable speed grid connected wind turbine, Energy Conversion and Management 79 (2014) 281–288.
[31] T. Ramesh, A. K. Panda, S. S. Kumar, Type-2 fuzzy logic control based mras speed estimator for speed sensorless direct torque and flux control of an induction motor drive, ISA transactions 57 (2015) 262–275.
[32] R. Cárdenas, R. Peña, J. Clare, G. Asher, J. Proboste, Mras observers for sensorless control of doubly-fed induction generators, Power Electronics, IEEE Transactions on 23 (3) (2008) 1075–1084.
[33] A. Chaiba, R. Abdessemed M. L. Bendaas, L. A "Hybrid Intelligent Control based Torque Tracking approach for Doubly Fed Asynchronous Motor (DFAM) drive", Journal of Electrical Systems. 262-272. 2012.
[34] C. Elmas, O. Ustun, H. H. Sayan, A neuro-fuzzy controller for speed control of a permanent magnet synchronous motor drive, Expert Systems with Applications 34 (1) (2008) 657–664.
[35] Gökbulut, M., Dandil, B; & Bal, C., A hybrid neuro-fuzzy controller for brushless DC motors. Lecture Notes in Computer Science, 3949. 125-132.
[36] K. Kouzi, M. Nait-Said, M. Hilairet, É. Berthelot, A fuzzy sliding-mode adaptive speed observer for vector control of an induction motor, in: IEEE International Conference on Industrial Electronics IECON, 2008.
[37] R. Andreoli de Marchi, P. S. Dainez, F. J. Von Zuben, E. Bim, A multilayer perceptron controller applied to the direct power control of a doubly fed induction generator, Sustainable Energy, IEEE Transactions on 5 (2) (2014) 498–506.
[38] Y. Daili, J.-P. Gaubert, L. Rahmani, Implementation of a new maximum power point tracking control strategy for small wind energy conversion systems without mechanical sensors, Energy Conversion and Management 97 (2015) 298–306.
[39] Y. Bekakra, D. B. Attous, Dfig sliding mode control driven by wind turbine with using a svm inverter for improve the quality of energy injected into the electrical grid, ECTI Transactions on Electrical Engineering, Electronics, and Communications 11 (1) (2014) 36–75.
[40] G. Abad, J. Lopez, M. Rodríguez, L. Marroyo, G. Iwanski, Doubly fed induction machine: modeling and control for wind energy generation, Vol. 85, John Wiley & Sons, 2011.
[41] Y. Lei, A. Mullane, G. Lightbody, R. Yacamini, Modeling of the wind turbine with a doubly fed induction generator for grid integration studies, Energy Conversion, IEEE Transactions on 21 (1) (2006) 257–264.
[42] A. Chaiba, R. Abdessemed, M. Bendaas, A. Dendouga, Performances of torque tracking control for doubly fed asynchronous motor using pi and fuzzy logic controllers, Journal of Electrical Engineering (2).